



OPEN

# Regional precipitation variability in East Asia related to climate and environmental factors during 1979-2012

SUBJECT AREAS:

ATMOSPHERIC  
DYNAMICS

HYDROLOGY

Received  
28 January 2014Accepted  
11 June 2014Published  
17 July 2014Yinyin Deng<sup>1</sup>, Tao Gao<sup>1,2</sup>, Huiwang Gao<sup>1</sup>, Xiaohong Yao<sup>1</sup> & Lian Xie<sup>1,3</sup>

<sup>1</sup>Key Laboratory of Marine Environment and Ecology, Ministry of Education, Ocean University of China, Qingdao 266100, China, <sup>2</sup>Department of Resources and Environmental Sciences, Heze University, Heze, 274000, China, <sup>3</sup>Department of Marine, Earth and atmospheric Sciences, North Carolina State University, Raleigh NC 27695-8208, USA.

Correspondence and requests for materials should be addressed to H.W.G. (hwgao@ouc.edu.cn)

This paper studies the inter-annual precipitation variations in different regions of East Asia from oceans to interior areas in China during 1979 – 2012. The results computed by Empirical Orthogonal Functions (EOF) demonstrate that the annual precipitation changes are mainly related to the El Niño-Southern Oscillation, East Asian summer monsoon and aerosols. We also found that the increased Sea surface temperature (SST) could explain the precipitation changes over the Northwest Pacific in the dry season (Oct. – May) and the East China Sea and the South China Sea in the rainy season (Jun. – Sep.). The precipitation changes over the ocean unexplained by SST were likely due to the water vapor transport dominated by dynamic factors. With the increased SST, the moisture transported from oceans to interior land was likely redistributed and caused the complicated regional variability of precipitation. Moreover, the impacts of aerosols on cloud and precipitation varied with different pollution levels and different seasons.

Ocean precipitation accounts for approximately 80% of global precipitation and plays a vital role in the Earth's climate system<sup>1</sup>. Its variations can directly impact the intensity of the global hydrological cycle and the redistribution of precipitation over land and sea<sup>2</sup>. Enormous efforts have been made to improve the understanding of how ocean precipitation responds to warming climate<sup>3–6</sup>. Globally, precipitation increases in equatorial rain bands; decreases in subtropics as greater tropical convection in the rising branch of the Hadley circulation will lead to enhanced subsidence in the subtropics; and increases in high-latitudes due to increase in moisture transport<sup>7–9</sup>. However, the response of precipitation to the global warming varies regionally. For the tropical ocean, two viewpoints have coexisted in interpreting precipitation changes, i.e., one predicts intensified rainfall in presently rainy regions (wet-get-wetter)<sup>3,6</sup>, and the other suggests that increased precipitation would occur where the sea surface temperature (SST) rises more (warmer-get-wetter)<sup>4,5</sup>. Huang et al.<sup>7</sup> recently proposed that the two kinds of mechanisms above are not contradictory, but complementary, i.e., the variability of the annual mean precipitation over the tropical ocean follows warmer-get-wetter, whereas the seasonal-mean precipitation follows the wet-get-wetter mechanism. Moreover, the precipitation in the mid- and high latitudes has increased by about 0.5 to 1% per decade, except over East Asia<sup>9</sup>. What causes the exception in East Asia is still poorly understood<sup>10,11</sup>.

East Asia is a region experiencing huge human population and rapid economic growth in recent years. The precipitation in East Asia can be affected by several climatic factors. El Niño–Southern Oscillation (ENSO), a coupled ocean-atmosphere tropical Pacific phenomenon, is known to affect regional precipitation by altering the tropical cyclones in different ways<sup>12</sup>. As the strongest signal of inter-annual climate variability, ENSO may be becoming more frequent in the warming climate (cycle from 7–8 years to 3–4 years)<sup>13</sup>. In addition, the monsoons, i.e., East Asian summer monsoon (EASM), the South Asian summer monsoon (SASM), the Indian summer monsoon (ISM) and the western North Pacific summer monsoon (WNPSM), are also cyclical factors greatly affecting regional precipitation in Asia and all have a seasonal cycle. Recent report indicates that the EASM has experienced significant weakening after 1970s, thus leading to a decrease of precipitation in north China<sup>14</sup>. The SASM is also weakening and is found to be influenced by the increase of anthropogenic aerosols<sup>15</sup>. Unlike ENSO, EASM and SASM etc., SST experienced a monotonic increase. The increase is proposed to have a strong control



on the spatial variation of precipitation<sup>13</sup>, and the relationship between the warming SST and precipitation is nonlinear<sup>16</sup>.

The anomalous changes of regional precipitation under global warming may not be solely due to the climate variabilities such as ENSO, monsoon and SST changes. Atmospheric aerosols can also play a role<sup>15</sup>, which are highly varying with time and space. They can impact regional precipitation by affecting the cloud microphysics properties and even weakening the monsoons<sup>15</sup>. Moreover, atmospheric aerosols may partially offset the positive forcing due to greenhouse gases<sup>17</sup>. Asia, particularly China, has become one of the highest aerosol loading regions in the world. The increased summer floods in south China and droughts in north China have been associated with the increasing loadings of aerosols<sup>18</sup>.

The regional precipitation has a direct influence on agriculture activities and local economic and social development. Large uncertainties are still present on the forecast of regional precipitation even for the most advanced models<sup>11,20</sup>, although the responses of precipitation to ocean warming has been extensively studied on the global scales<sup>5,19</sup>. An in-depth analysis of long-term variability of regional precipitation in East Asia and related climatic and environmental factors are crucial to reveal the intrinsic mechanisms and would benefit for forecasting the future. In view of this, the objectives of this study are to characterize inter-annual variability of precipitation over various monsoon-influenced zones in East Asia during 1979–2012 and to improve the understanding of inhomogeneity of regional precipitation changes related to ocean warming. In addition, we will pay particular attention to the influences of the cyclical factors (ENSO and the monsoon circulations), aperiodic climate factor (SST) and regional factors (aerosols and clouds) on the changes of precipitation over our study zone in the last three decades.

## Methodology

**Data sources.** The datasets used in this study include: 1) version 2.2 monthly average Global Precipitation Climatology Project (GPCP) products (available at <http://precip.gsfc.nasa.gov/>) on a  $2.5^\circ \times 2.5^\circ$  grid. GPCP is the combination of a variety of micro-wave data, infrared data and the surface rain-gauge data<sup>21</sup>. GPCP precipitation data has been extensively used for the precipitation analysis in the tropics and mid-latitudes<sup>21,22</sup>. 2) ERSST (version 3b) which is the US National Oceanic and Atmospheric Administration's (NOAA) Extended Reconstruction of SST dataset (<http://www.esrl.noaa.gov/psd/>), with a  $2.0^\circ \times 2.0^\circ$  resolution<sup>23</sup>. The ERSST analysis is based on the available Global Telecommunications System (GTS) ship and buoy observations from the International Comprehensive Ocean–Atmosphere Data Set (ICOADS). 3) NOAA Niño-3.4 index which is defined as the average SST anomalies over the Niño-3.4 region ( $5^\circ\text{S}–5^\circ\text{N}$ ,  $170^\circ\text{E}–120^\circ\text{W}$ ). The SST variability in the Niño-3.4 region is reported to have a strong effect on shifting rainfall in the western Pacific and is often used as an ENSO index<sup>24</sup>. 4) Four monsoon indices are used in this study to examine the relationship between the precipitation and monsoons, such as EASMI, SASMI, IMI and WNPMI. The definition of the four monsoon indices has been listed in Table 1. 5) Monthly average Moderate-resolution Imaging Spectroradiometer (MODIS) Level 3, Collection 5 datasets onboard the Terra satellite (<http://ladsweb.nascom.nasa.gov/data/search.html>). It has a spatial resolution of

$1.0^\circ \times 1.0^\circ$ . The specific parameters used in this study include aerosol optical depth (AOD) at 550 nm, fine mode (aerodynamic diameter ( $D_p$ )  $< 1 \mu\text{m}$ ) AOD and clouds fraction (CF), cloud effective radius (CER). MODIS aerosol products can monitor the temporal and spatial characteristics of the global aerosol field over land and ocean. In particular, the MODIS aerosol products over China have been extensively validated using the Aerosol Robotic Network (AERONET)<sup>29</sup> and the Chinese Sun Haze meter Network (CSHNET) data<sup>30</sup>. 6) Global reanalysis data sets provided by National Centers for Environmental Prediction/National Center for Atmospheric Research (NCEP/NCAR) for the period 1979–2012 are used to estimate the terms of the atmospheric water vapor transport<sup>31</sup>. The physical variables used in this study include the monthly average specific humidity, and the meridional and zonal wind components at eight standard pressure levels: 1000, 925, 850, 700, 600, 500, 400, and 300 hPa. The vertically-integrated moisture flux can be expressed as

$$\vec{Q} = \frac{1}{g} \int_0^{p_s} q \vec{V} dp, \quad (1)$$

and the moisture flux divergence can be represented as

$$\nabla_p \cdot (\vec{V}q/g) = \frac{\partial}{\partial x} (\vec{V}q/g), \quad (2)$$

where  $\vec{Q}$  is the vertically integrated moisture flux,  $q$  is specific humidity,  $\vec{V}$  is the horizontal wind vector,  $p$  is the pressure,  $p_s$  is the surface pressure,  $g$  is the acceleration due to gravity, and  $\nabla_p \cdot (\vec{V}q/g)$  is the divergence of the integrated moisture flux.

**Study areas.** Our study regions include both the oceans and the continents in East Asia (Fig. 1). The oceanic zones contain the Yellow Sea (YS,  $120^\circ\text{E}–126^\circ\text{E}$ ,  $32^\circ\text{N}–39^\circ\text{N}$ ), East China Sea (ECS,  $117^\circ\text{E}–129^\circ\text{E}$ ,  $25^\circ\text{N}–34^\circ\text{N}$ ), South China Sea (SCS,  $106^\circ\text{E}–121^\circ\text{E}$ ,  $3^\circ\text{N}–22^\circ\text{N}$ ) and Northwest Pacific (NP,  $122^\circ\text{E}–147^\circ\text{E}$ ,  $1^\circ\text{N}–35^\circ\text{N}$ ). Over continents, we focus on the coastal areas within 250 km from YS, ECS and SCS. Over the coastal areas the summer moisture is mainly from the ocean, especially the coastal areas of ECS and SCS, but the loadings of atmospheric aerosols are much higher compared to those in the marine atmosphere. For inter-comparison, the precipitation changes over the monsoon-influenced regions in China are also analyzed. These regions are interior lands, but the moisture is partially influenced by the monsoons. The interior lands are further divided into north China and south China according to the traditional climate regionalization. The Qinling-Huaihe Line is the demarcation line between south and north China<sup>32</sup>.

## Methods

Empirical orthogonal functions (EOF) and the Pearson product-moment correlation analysis (PCC) are used for data interpretation. The EOF is a statistical method that can extract the dominant modes of change from a time-dependent two-dimensional dataset. The EOF analysis gives spatial patterns of each mode and the time series of the loadings of the modes. The EOF spatial patterns are eigenvectors, which are orthogonal so that the leading EOFs describe the spatially coherent pattern that maximizes its variance<sup>33</sup>. The PCC is usually used to measure the degree of linear relationship between two variables<sup>34</sup>. The correlation will be noted when the statistical significance is equal to or exceeds the 95% confidence level.

**Table 1** | The definition of four monsoon indices used in this study

Monsoon Indices	Definition	Time domain	Reference
East Asian Summer Monsoon Index (EASMI)	U850( $110^\circ–140^\circ\text{E}$ , $10^\circ–40^\circ\text{N}$ )	June to August	25,26
South Asian Summer Monsoon Index (SASMI)	U850( $35^\circ–97.5^\circ\text{E}$ , $5^\circ–22.5^\circ\text{N}$ )	June to September	25,26
Indian Monsoon Index (IMI)	U850( $40^\circ–80^\circ\text{E}$ , $5^\circ–15^\circ\text{N}$ )-U850( $70^\circ–90^\circ\text{E}$ , $20^\circ–30^\circ\text{N}$ )	June to September	27,28
Western North Pacific Monsoon Index (WNPMI)	U850( $100^\circ–130^\circ\text{E}$ , $5^\circ–15^\circ\text{N}$ )-U850( $110^\circ–140^\circ\text{E}$ , $20^\circ–30^\circ\text{N}$ )	June to September	27,28

Note: U850 is defined as the area-averaged dynamical normalized seasonality (DNS) zonal wind anomalies at 850 hPa.

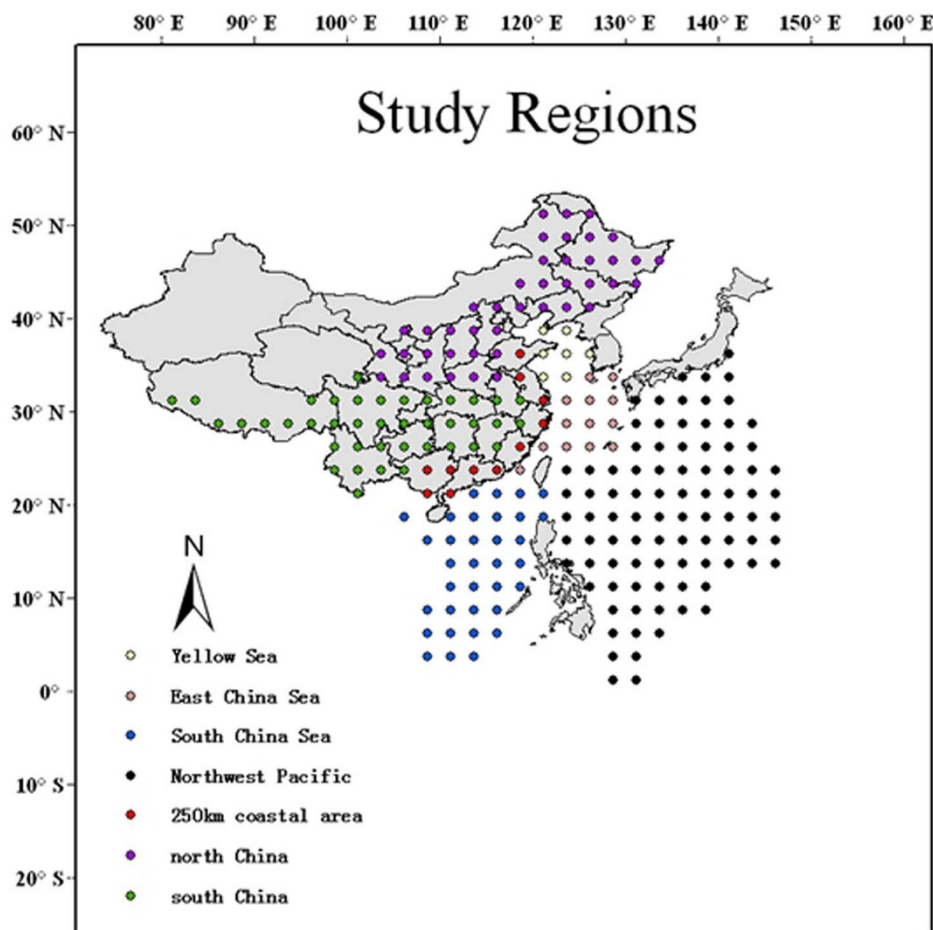


**Figure 1** | Map of the study regions (the grid points for precipitation data reading are marked in different colors, representing different areas). The map in the figure was created by D.Y. using Arcgis 9.3.

To measure the atmospheric water-holding capacity as a function of local  $T$ , we use an approximation to the Clausius–Clapeyron relation of the form:

$$e_s = A \exp[BT/(C+T)], \quad (3)$$

where  $e_s$  is the saturated vapor pressure (kPa),  $T$  is the surface air temperature ( $^{\circ}\text{C}$ ) and the constants  $A$ ,  $B$ , and  $C$  have the values 0.6108, 17.27, and 237.3, respectively<sup>35</sup>. Since marine air temperature has a good agreement with SST in daily average over the majority of large ocean regions, SST data can be used as a proxy for marine air temperature. This is especially true for this study as the time resolution of SST used in this study is monthly mean<sup>36</sup>. We compute the increasing rate of the calculated water-holding capacity per  $^{\circ}\text{C}$  SST ( $\Delta W/\Delta T$ ) using the formula:

$$\frac{\Delta W}{\Delta T} = (e_{s2012} - e_{s1979})/e_{s1979}/(T_{2012} - T_{1979}), \quad (4)$$

$e_{s1979}$  and  $e_{s2012}$  indicate the  $e_s$  in 1979 and 2012,  $T_{1979}$  and  $T_{2012}$  stand for the SST in 1979 and 2012, respectively. The net increase of precipitation by the net increase of SST ( $\Delta P/\Delta T$ ) is computed with the formula:

$$\frac{\Delta P}{\Delta T} = (P_{2012} - P_{1979})/P_{1979}/(T_{2012} - T_{1979}), \quad (5)$$

$P_{1979}$  and  $P_{2012}$  are the precipitation in 1979 and 2012. The units of  $\Delta W/\Delta T$  and  $\Delta P/\Delta T$  are both  $\%/^{\circ}\text{C}$ . Globally, this equation determines that the water-holding capacity of the atmosphere increases by about 7% for every  $1^{\circ}\text{C}$  rise in temperature from 1900 to 2002<sup>37</sup>.

## Results and Discussion

**Regional variability of precipitation in East Asia related to cyclical factors.** To explore temporal and spatial distributions of annual precipitation variations in East Asia during 1979–2012, EOF analysis is performed on annual precipitation anomaly fields. Only the first three EOFs and corresponding principal components (PCs) (Fig. 2) have passed the North test<sup>33</sup> and they account for 52.8% of the

variance. The three EOFs and corresponding PCs are discussed in terms of correlations between the PCs of each mode and the possible influencing factors (Niño-3.4 index, EASMI, SASMI, ISMI, WNPSMI and AOD, CER, CF). The first EOF accounts for 33% of the anomaly variance (Fig. 2a) and shows a negative phase over the NP, the SCS, the north YS and parts of the north China. The variation of the precipitation is the product of the space field and time field of the EOF. The corresponding PC1 (Fig. 2d) has a decreasing tendency from 1979 to 2012, implying that the precipitation in these regions has increased in the past three decades. The increase is more obvious over the NP and SCS than over the north YS and parts of the north China. A significant correlation ( $r = 0.53$ ) is obtained between the PC1 and the Niño-3.4 index from non-trend interannual variations, indicating that the first mode largely reflects ENSO-related trend variations. Smith et al.<sup>38</sup> and Trenberth et al.<sup>39</sup> have analyzed the global precipitation using EOF and also attributed the first mode to the influence of ENSO on the basis of correlations between the PCs and the Niño index.

The second mode (Fig. 2b) seems to be associated with the ENSO as well<sup>38,39</sup>, except that PC2 shows a significant negative correlation ( $r = -0.58$ ) with the Niño-3.4 index. Furthermore, PC2 also shows a negative correlation to the WNPSMI ( $r = -0.62$ ) and the EASMI ( $r = -0.4$ ), but has a significant positive correlation with CF ( $r = 0.64$ ). There is a weaker East Asian monsoon circulation and a delayed onset with the warmer SST anomalies in the region of Niño-3.4<sup>40</sup>. Thus, the indices are not independent from each other and all have a significant correlation with PC2. Excluding the two ENSO-related abnormal years, i.e., 1999 (flood year) and 2005 (drought year), the PC2 shows a slight decrease before 1995, but then a slight increase.

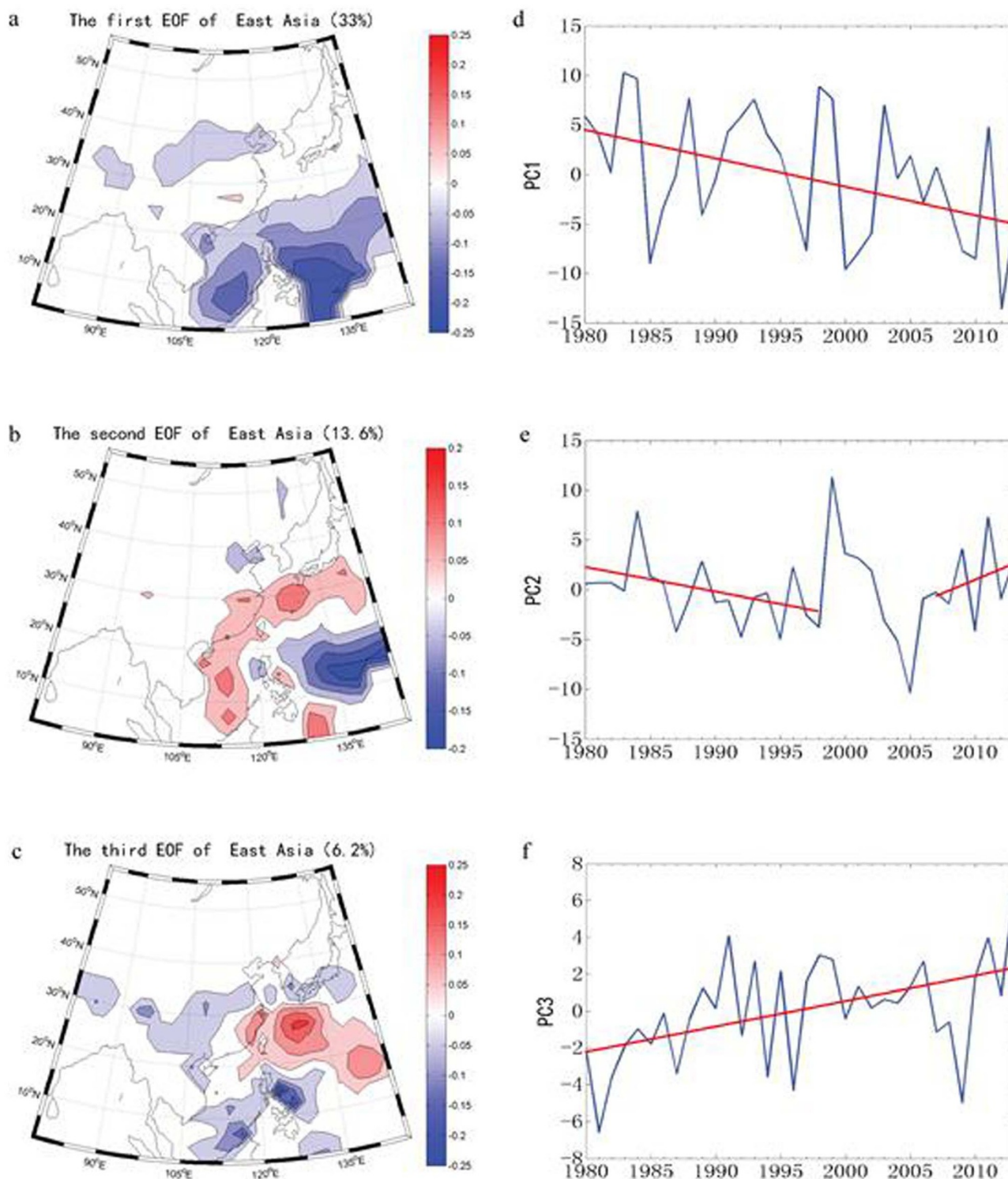


**Figure 2** | The first three EOFs (left panel, (a), (b), (c)) and principal components (right panel, (d), (e), (f)) for annual precipitation of study areas during 1979–2012, and the red line in the figure indicates the linear fitting of the principal components. The maps in the figure were created by D.Y. using Matlab 2011b.

The decreasing trend in the southern part of the NP in the second mode could be partly associated with the reduced water vapor amount owing to the weakening of EASM, especially the WNPSM<sup>14</sup>. There is an eastward-movement of the westernmost 588-dagpm contours of the 500 hPa geo-potential height field over western Pacific (approximately 134°E before 1993 and 132°E after 1994) (also see Supplementary Fig. S1), which indicates that the WNPSM is weakening. Although the water vapor amount also

reduced over the ECS, SCS and their coastal areas (Figs. 3 and 4), the precipitation over these areas got enhanced. That can occur because the precipitation is determined by both local evaporation amounts and the moisture fluxes from remote moisture source regions.

The third mode (Fig. 2c) accounts for 6.2% of the total variance and the corresponding PC3 (Fig. 2f) exhibits an obvious increasing trend. No significant correlations are found between PC3 and Niño-

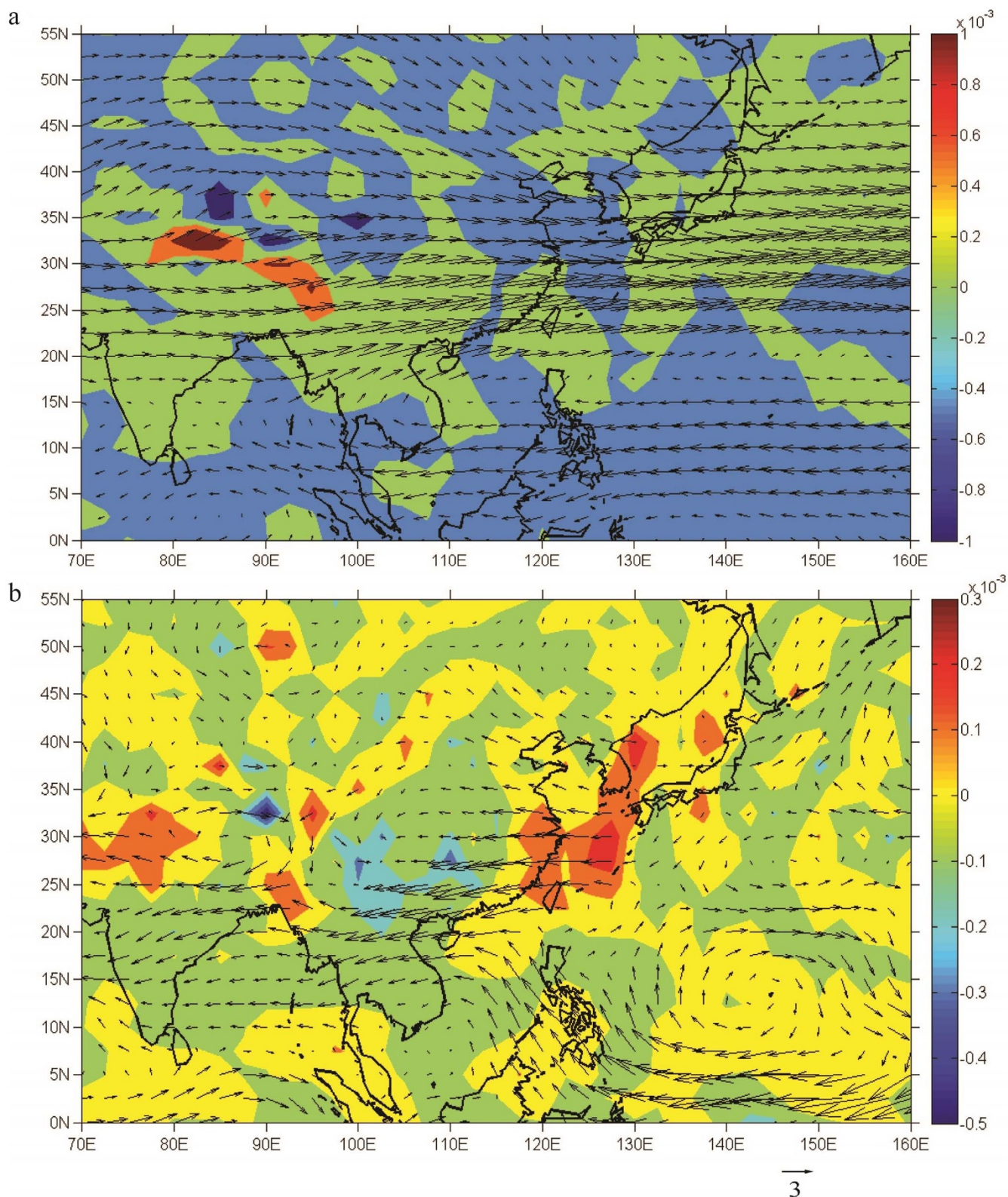


**Figure 3** | The vertically integrated mean water vapor transport over our study areas in the dry season (Oct.–May). (a), the vertically integrated mean water vapor transport for 1979–1993. (b), the difference of the vertically integrated mean water vapor transport between 1979–1993 and 1998–2012. The arrow key is standing for the water vapor flux and the color shading is representing the water vapor flux divergence. The unit is  $\text{g}/(\text{cm}^2 \cdot \text{hPa} \cdot \text{s})$  for the water vapor flux and  $\text{g}/(\text{cm}^2 \cdot \text{hPa} \cdot \text{s})$  for the water vapor flux divergence. The turning time chosen for the comparison is the shift time of the SST over the four seas, i.e., 1993–1998 in the dry season. The maps in the figure were created by G.T. using Matlab 2011b.

3.4 index or between PC3 and EASMI, but PC3 has a significant correlation with total AOD ( $r = -0.64$ ). This suggests that the third mode is possibly related to the atmospheric aerosols. Three modes

are also reported in EOF analysis of global precipitation by Gu and Adler et al.<sup>41</sup>. In which, two modes appears to be related to ENSO, similar to our study. However, they attributed the third EOFs to some

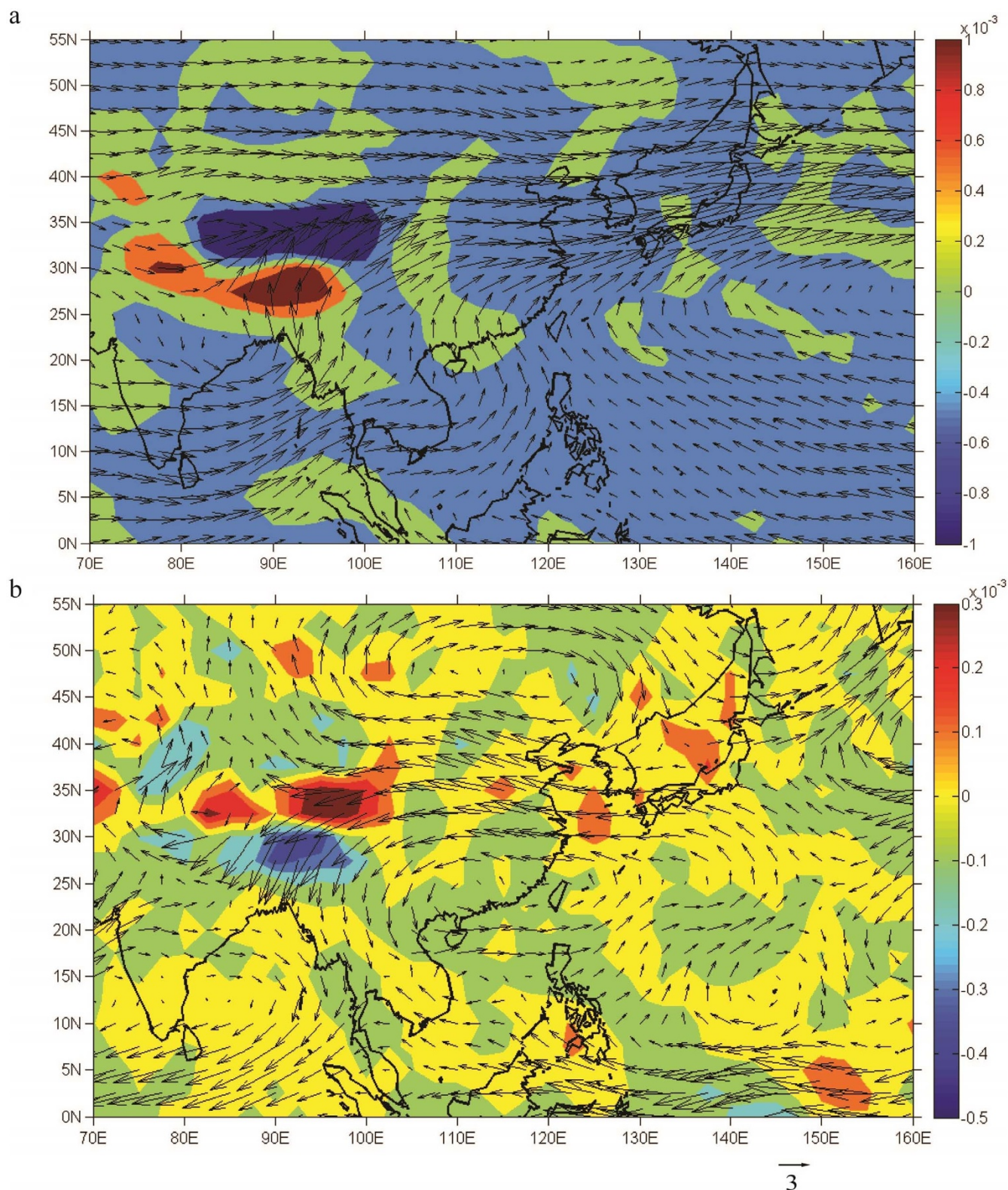


**Figure 4** | Same as Fig. 3 but for the rainy season (June–Sep.), and the turning time is 1994. The maps in the figure were created by G.T. using Matlab 2011b.

aspects of regional precipitation changes. The third EOFs in this study shows a stronger increase in NP, but a weaker decrease in the south China and YS. We will discuss the relationships between precipitation and atmospheric aerosols in a later section.

**Regional variability of ocean precipitation related to SST.** For oceans, the elevated SST is the most direct indicator of global

warming. Climate models and satellite observations both indicate that the total amount of water in the atmosphere increased at a rate of 7% per kelvin of surface warming and the observed precipitation also exhibited an increasing rate of 6% per kelvin of surface warming over the past two decades<sup>19</sup>. Westra et al.<sup>42</sup> reported that the median intensity of extreme precipitation changed significantly in proportion to changes in global mean temperature



at a rate between 5.9% and 7.7% per kelvin. The larger moisture holding capacity of air in a warmer climate can cause more precipitation. With increasing global air temperature, the thermodynamic component associated with an increase of water vapor generally shows a positive contribution to precipitation changes<sup>6</sup>. However, the dynamic component due to the change in atmospheric motion could reduce or increase precipitation, depending on locations<sup>7–9,43</sup>.

We first examine the variability of SST and then examine possible relationship between SST and precipitation in the dry and rainy seasons separately. The homogeneity tests can find out the qualitative change of the dataset in the time series analysis by computing the variances<sup>44</sup>. An obvious shift during 1993–1998 detected by the homogeneity tests occurs both in the dry and rainy seasons (Fig. 5) indicates that the substantive change of the precipitation over the four oceans take place in 1993–1998. This shift appears to be associated with a climate regime shift in the Pacific basin. Bond et al.<sup>45</sup> reported a similar SST shift in 1998/99 over the western and central

NP which was characterized by a meridional seesaw of SST anomalies. In the dry season, the shift over the YS, ECS, SCS and NP occurs in 1993/1994, 1996/1997, 1996/1997 and 1997/1998, respectively. For rainy season, the shifts all occur in 1993/1994 regardless of the locations of our study oceans. The shifts occur earlier in oceanic regions are closer to the continent. The precise reason for this shift remains unclear. After the SST jump, a downward trend is observed for the dry season SST at a rate of 0.22–0.33°C per decade over our oceanic regions, whereas in the rainy season SST fluctuates with no clear trend. The shift of the SST in the dry or rainy season may have an influence on the precipitation, even though they are not coincident.

To further study the impact of the SST on precipitation, we divided the net increase of precipitation by the net increase of SST ( $\Delta P/\Delta T$ ) and compared with the increasing rate of the calculated water-holding capacity per °C SST ( $\Delta W/\Delta T$ ). In the dry season, the ratios of  $\Delta P/\Delta T$  are  $-0.02 \pm 0.003\%/^{\circ}\text{C}$  (mean  $\pm$  standard deviation) over the YS,  $-14 \pm 2\%/^{\circ}\text{C}$  over the ECS,  $75 \pm 4.4\%/^{\circ}\text{C}$  over the SCS and  $23 \pm$

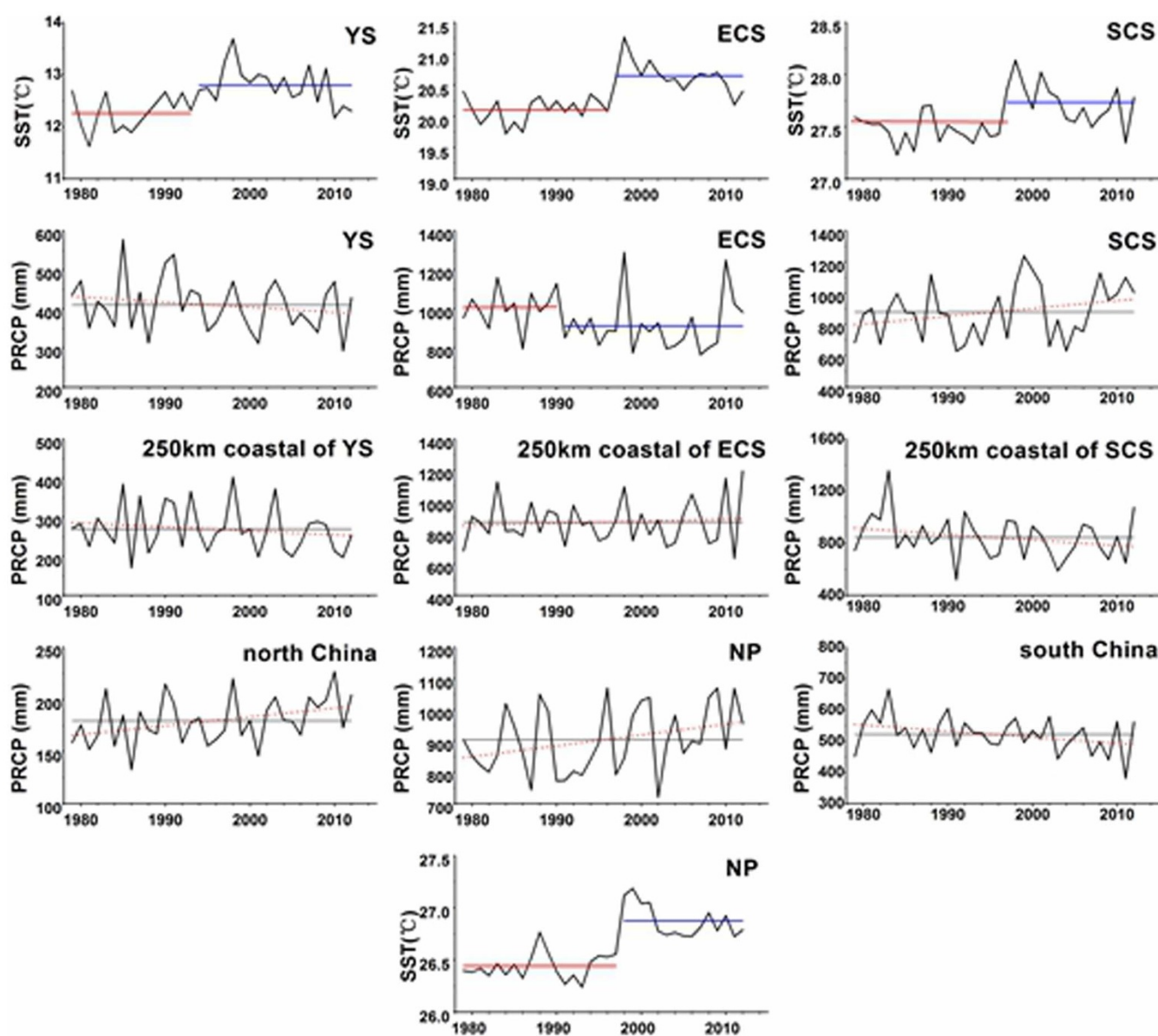


**Figure 5** | Comparison between the dry season (Oct.–May) precipitation and SST over Yellow Sea, East China Sea, South China Sea, the 250 km coastal areas adjoining to three seas, the south China, the north China, and Northwest Pacific during 1979–2012. The red dot line stands for the linear trend of the precipitation. The red line in the figure indicates the mean of the SST or precipitation before the shift tested by the homogeneity test with the Excel 2010, while the blue line indicates the means of the SST or precipitation after the shift.





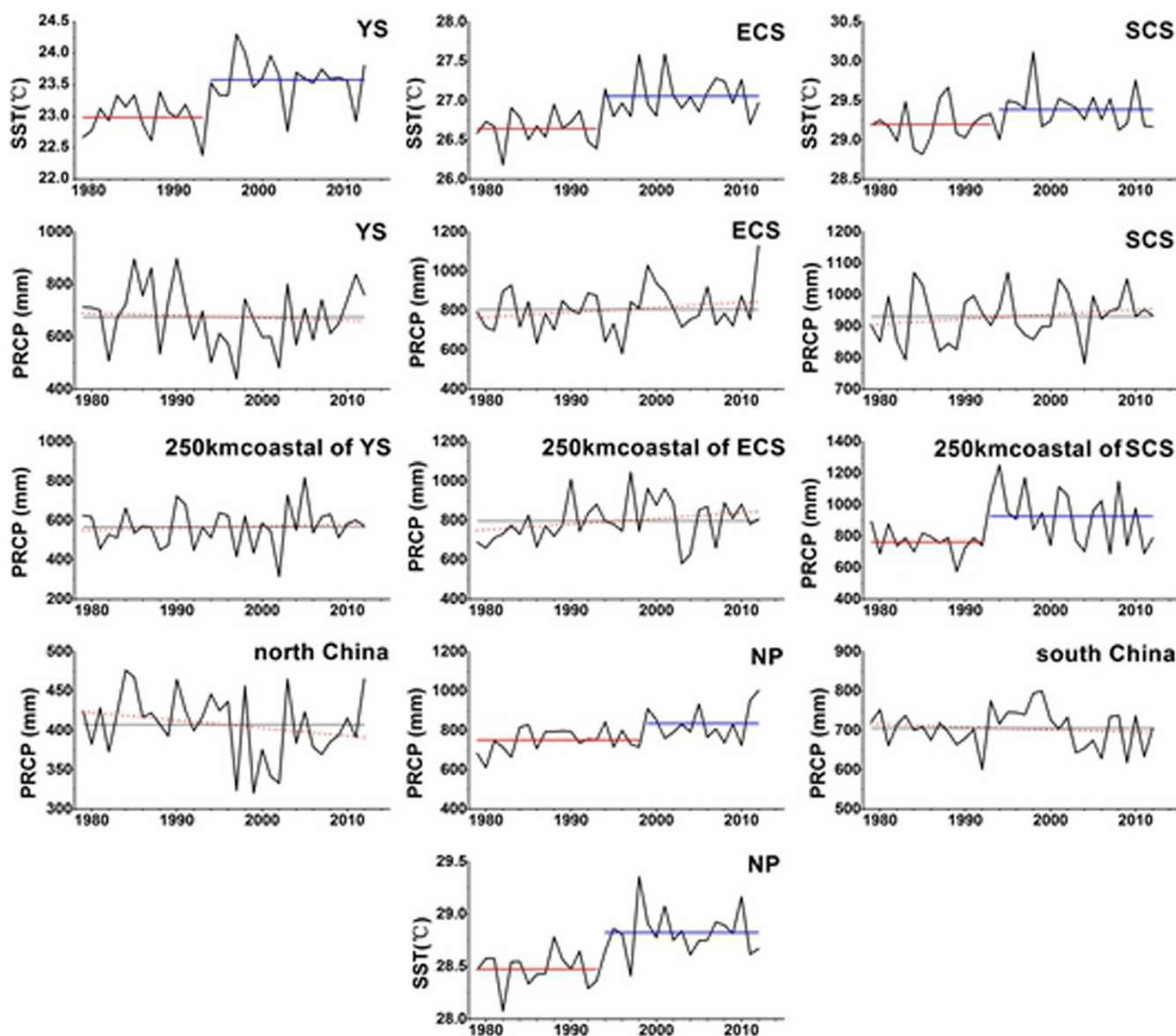


Figure 6 | Same as Fig. 5 but for the rainy season (June–Sep.).

moisture from the SCS being transported to inland areas through the water vapor passing along the SCS (see Fig. 3).

In the rainy season (Fig. 6), the coastal area adjoining to the YS has a slight increase in precipitation, yet the precipitation over the north China decreases by  $12 \pm 1.3$  mm per decade. More droughts during summer has been reported in north China since the late 1990s<sup>48</sup>. The physical connections, if any, among precipitation decrease over the YS, increase over the coastal area adjacent to the YS and decrease over the north China need more modeling studies which are beyond the scope of this study. The rainy season precipitation of the coastal area adjacent to the ECS exhibits an increase with the rate  $30 \pm 1.2$  mm per decade and the rate is almost the same as that over the ECS. The supply of water vapor from the SCS and the NP to ECS and its coastal areas is greatly reduced (Fig. 4). The increase over the ECS is likely due to its increasing moisture holding capacity of air as mentioned earlier. The same reason could also be true for the increase of precipitation over the coastal area adjacent to the ECS. The rainy season precipitation over the coastal area adjacent to the SCS has a shift in 1993/1994 and the shift matches the rainy season SST shift in the SCS. The rainy season precipitation over the coastal area from the SCS increases by  $40 \pm 1.7$  mm per decade, which is much larger than

the  $12 \pm 6.3$  mm per decade increase over the SCS in the same season. The precipitation over the monsoon-influenced zones in south China decreases by  $-10 \pm 2.5$  mm per decade. The moisture transported by cross-equatorial flow and South Asian monsoon to the SCS were largely weakened in the rainy season (see Fig. 4), also supporting that the increase of the precipitation over the SCS may be due to the thermodynamic components. Moreover, Nanling Mountains can partially block the moisture from the SCS in the rainy season, leading to more precipitation in the windward side and less precipitation in the leeward side. Overall, with the increasing SST, moisture transport from oceans to interior land is likely redistributed, causing the complicated variability of precipitation over different regions in the dry and rainy seasons.

**Variability of precipitation related to aerosols.** Aerosols can act as cloud condensation nuclei (CCN) and have an influence on regional precipitation<sup>49</sup>. The effects of aerosols on the precipitation is mostly to suppress it<sup>9</sup>, but they can sometimes enhance it<sup>49</sup>. Using a combination of observations and modelling results, Yi et al.<sup>51</sup> proposed that there is a negative correlation between AOD and precipitation over land and a positive correlation over ocean. The

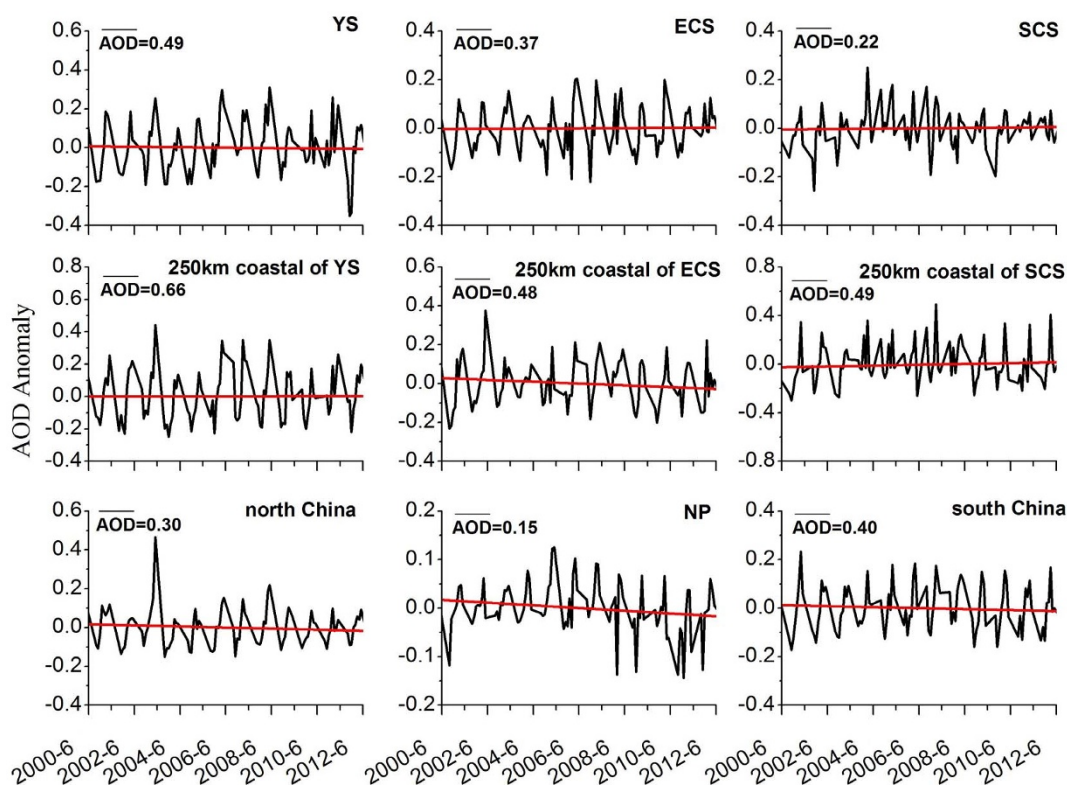


**Figure 7** | Time series of the monthly AOD anomaly during 2000–2012 over the study areas in the dry season (Oct.–May), and the red line in the figure indicates the linear fitting of the AOD anomaly, and AOD represents the average of the AOD value in different areas.

AOD data are only available after 2000, and thus our study is confined to 2000–2012, with results shown in Figs. 7 and 8. In the dry season, the values of AOD are  $0.5 \pm 0.1$  over the YS,  $0.4 \pm 0.1$  over the ECS,  $0.2 \pm 0.08$  over the SCS,  $0.2 \pm 0.05$  over the NP while

they are  $0.7 \pm 0.2$  over the coastal area adjoining the YS,  $0.5 \pm 0.1$  over the coastal area adjacent to the ECS,  $0.5 \pm 0.2$  over the coastal area adjacent to the SCS,  $0.3 \pm 0.1$  over north China, and  $0.4 \pm 0.1$  over south China, respectively (Figs. 7 and 8). Tang et al.<sup>52</sup> classified

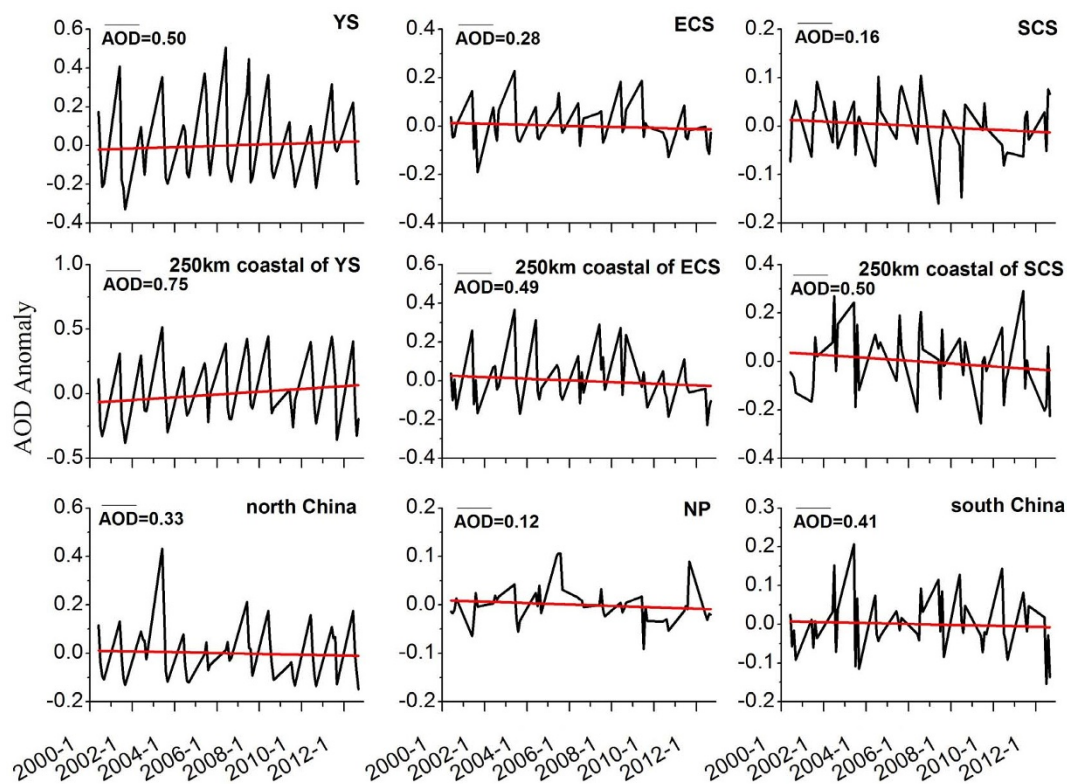


**Figure 8** | Same as Fig. 7 but for the rainy season (June–Sep.).



**Table 3 |** The correlations between the precipitation and related factors (CF, CER, AOD, Fine-Mode (aerodynamic diameter ( $D_p$ ) < 1  $\mu\text{m}$ ) AOD and SST) from the NP to the interior China in the dry season (Oct.–May) and rainy season (June–Sep.) during 2000–2012. All the correlation coefficients are tested using the Pearson correlation test, the single asterisk is for  $P < 0.05$ , and the double asterisk is on behalf of  $P < 0.01$

		Dry Season					Rainy Season				
		CF	CER	AOD	Fine-Mode AOD	SST	CF	CER	AOD	Fine-Mode AOD	SST
PRCP	YS			0.33**	0.27**		YS	0.57**	0.31*		0.29*
	ECS		0.68**	0.29**	0.23*	0.21*	ECS	0.73**	0.31*		−0.65**
	SCS	0.75**	0.70**	−0.46**	−0.33**	0.51**	SCS	0.34*		0.40**	
	NP	0.48**	0.75**	−0.38**	−0.34**	0.68**	NP	0.72**			
	250 km YS			0.39**	0.24*		250 km YS	0.57**	0.28*		0.47**
	250 km ECS	0.57**	0.64**	0.34**	0.31**		250 km ECS	0.74**	0.30*	0.38**	
	250 km SCS	0.47**	0.67**				250 km SCS	0.72**	0.64**		−0.33*
	north China	−0.38**	−0.40**	0.31**	0.40**		north China	0.79**			0.41**
	south China	0.54**	0.83**	0.39**			south China	0.78**	0.83**		

AOD into three types: low (0–0.3), moderate (0.3–0.6), and high (0.6–0.9) pollution levels. According to the classification, the average value of AOD over the SCS, NP, and north China was low (Fig. 7). The average value of AOD in the coastal area adjacent to the YS was the highest and the area that had the highest emissions of  $\text{SO}_2$  in China<sup>53</sup>. The remaining AODs rank at the moderate level. In the rainy season, the values of AOD are  $0.5 \pm 0.2$  over the YS,  $0.3 \pm 0.08$  over the ECS,  $0.2 \pm 0.06$  over the SCS,  $0.8 \pm 0.3$  over the coastal area adjacent to the YS,  $0.5 \pm 0.1$  over the coastal area adjacent to the ECS,  $0.5 \pm 0.1$  over the coastal area adjacent to the SCS,  $0.3 \pm 0.1$  over north China,  $0.1 \pm 0.04$  over the NP, and  $0.4 \pm 0.07$  over south China. The ECS, SCS, and NP are all clean areas by this classification. When the time series of AOD anomaly is examined, AOD anomaly first increased and then decreased over the SCS and NP in the dry season during 2000–2012, and the turning point was around 2006. No clear temporal trend for AOD anomaly is exhibited over other regions. In the rainy season the increasing trend is found only over the YS and the coastal area adjacent to the YS. The AOD anomaly over the NP increased first and then decreased after 2006, similar to the change in the dry season. The other areas exhibit a decreasing trend in AOD anomaly.

To further investigate the role of aerosols on the cloud microphysical properties and the effects of aerosols and clouds on precipitation, the correlations among the MODIS satellite AOD, CER and CF are computed for 2000–2012 (Table 2) as well as the correlations between the precipitation and AOD, CER, CF in the same regions (Table 3). From the perspective of aerosols, the atmosphere over the SCS and the NP is relatively clean, the coast areas adjacent to the YS suffers from severe particulate pollution, while the remaining study regions are moderate. In the relatively clean atmosphere, more aerosols are usually accompanied by the smaller CER, less CF and suppression of precipitation in the dry season. Rosenfeld et al.<sup>49</sup> pointed out that the fewer aerosol droplets, combining with the adequate moisture caused by the increasing SST, could make CCN grow and drop to the ocean surface quickly. The hypothesis can explain the negative correlations between AOD and other factors (i.e., precipitation, CER and CF) over the SCS and NP. For the rainy season, more aerosols are generally associated with smaller CER in the clean areas, but have no significant correlation with the precipitation. The summer monsoons may have a strong influence on the precipitation over the SCS and NP in the rainy season, overwhelming the effects of aerosols. With the adequate water vapor transported by the summer monsoons, greater CF is associated with more precipitation in the rainy season (Table 3). For the severe pollution area with high AOD loadings, i.e., the coastal area adjoining the YS, more aerosols and bigger CER probably promotes precipitation in both the dry and rainy season. Traditionally, excessive aerosols combining with the

increasing water vapor may form a large number of smaller CCN, prolonging the lifecycle of the cloud, and reducing the precipitation<sup>49</sup>. However, Koren et al.<sup>50</sup> recently proposed that excessive aerosols combining with high water vapor can sometimes enhance precipitation. For the remaining areas, the relationship among the precipitation, AOD, CER and CF are complicated and location-dependent. The best correlation of 0.83 between the precipitation and CER in the dry season occurs in south China. In the rainy season, the AOD has a positive correlation with the precipitation only in ECS and the coastal area adjacent to the ECS. The fine mode AOD is also used for correlation analysis. In theory, the fine mode aerosols should have better correlations with the cloud and precipitation than the total aerosols since fine mode particles usually have much higher number concentration. However, the correlations between the fine-mode AOD and the CER, CF, precipitation are very similar with the total AOD in both dry and rainy seasons. Overall, precipitation over the continents is likely affected more by aerosol and related CF and CER, while precipitation over the oceans is likely affected more by climate factors. As shown, the influence of aerosols on the precipitation varies with pollution level and season.

## Conclusions

This work combines statistics analysis of satellite data and diagnostic analysis of global reanalysis data sets for water vapor transport to study the regional precipitation changes from the Northwest Pacific (NP) to the interior of China under a warming climate and discusses the possible influence on the precipitation from four factors: ENSO (El Niño–Southern Oscillation), monsoons, SST (Sea surface temperature), and aerosols. Our results show that the first Empirical Orthogonal Functions (EOFs) of precipitation is mainly related to the ENSO, the second EOFs is associated with the ENSO, East Asian Summer Monsoon (EASM), and Western North Pacific Monsoon (WNPM), whereas the third EOFs is possibly dominated by the effect of aerosols. The role of South Asian Summer Monsoon (SASM) and Indian Monsoon (IM) on the precipitation in the monsoon-influenced zones is largely overwhelmed by the factors mentioned above, although the moisture from the Indian Ocean was one of the major sources for precipitation in East Asia.

The increased SST is an important cause for precipitation changes over the NP in the dry season and over the East China Sea (ECS) and South China Sea (SCS) in the rainy season. Over these oceanic regions, the ratios of the net increase of precipitation by the net increase of SST ( $\Delta P/\Delta T$ ) are almost the same as the ratios of the increasing rate of the calculated water-holding capacity per  $^\circ\text{C}$  SST ( $\Delta W/\Delta T$ ). For the SCS in the dry season and the NP in the rainy season, the ratios of  $\Delta P/\Delta T$  are 2–3 times  $\Delta W/\Delta T$  and dynamic components likely contributed more to the increased ratios of  $\Delta P/$



$\Delta T$ . The Subtropical high of the NP moving westward may cause additional increment of  $\Delta P/\Delta T$  ratios over SCS in the dry season while increase in southeast inflowing moisture along the southwest flank of the West Pacific Subtropical high may result in the additional increment of  $\Delta P/\Delta T$  ratios over the NP in the rainy season. However, the ratios of  $\Delta P/\Delta T$  are negative in both dry and rainy seasons over the YS, although the rates of  $\Delta W/\Delta T$  are highest among the four oceanic regions, suggesting that dynamic components and other factors overwhelm local thermodynamic components in those regions. In addition, the rainy season precipitation for coastal areas adjacent to the ECS exhibits an increase, with the rate almost same as that over the ECS. The rainy season precipitation over the coastal area adjacent to SCS has a shift in 1993/1994 and the shift matches the rainy season SST shift in the SCS. This evidence suggests that the increased SST not only affects ocean precipitation, but also the precipitation over the adjacent coastal areas.

In the relatively clean atmosphere, i.e., over the SCS and the NP, larger aerosol optical depth (AOD) are usually associated with the smaller cloud effective radius (CER), less clouds fraction (CF) and suppression of precipitation in the dry season. In the rainy season, no clear association was found for those regions. The coastal area adjacent to the YS is severely pollution area with high AOD loadings. Its larger AOD is associated with bigger CER and likely promotes the precipitation in both the dry and rainy seasons. For the remaining areas, the relationship among the precipitation, AOD, CER and CF are less clear.

- Schmitt, R. W. The ocean component of the global water cycle. *Rev. Geophys.* **33**, 1395–1409 (1995).
- Shin, D. B., Kim, J. H. & Park, H. J. Agreement between monthly precipitation estimates from TRMM satellite, NCEP reanalysis, and merged gauge-satellite analysis. *J. Geophys. Res.* **116**, D16105 (2011).
- Chou, C., Neelin, J., Chen, C. & Tu, J. Evaluating the “rich-get-richer” mechanism in tropical precipitation change under global warming. *J. Clim.* **22**, 1982–2005 (2009).
- John, O., Allan, R. P. & Soden, J. How robust are observed and simulated precipitation responses to tropical ocean warming? *Geophys. Res. Lett.* **36**, L14702 (2009).
- Xie, S. P. *et al.* Global Warming Pattern Formation: Sea Surface Temperature and Rainfall. *J. Clim.* **23**, 966–986 (2010).
- Held, M. & Soden, J. Robust responses of the hydrological cycle to global warming. *J. Clim.* **19**, 5686–5699 (2006).
- Huang, P. *et al.* Patterns of the seasonal response of tropical rainfall to global warming. *Nature Geosci.* **6**, 357–361 (2013).
- Lu, J., Vecchi, G. A. & Reichler, T. Expansion of the Hadley cell under global warming. *Geophys. Res. Lett.* **34**, L06805 (2007).
- Folland, C. K. *et al.* Climate Change 2001-The Scientific Basis: Contribution Of Working Group I To The IPCC Third Assessment Report, *Cambridge Univ. Press*. 99–181 (2001).
- Ramanathan, V., Crutzen, P. J., Kiehl, J. T. & Rosenfeld, D. Aerosols, climate, and the hydrological cycle. *Science*. **294**, 2119–2124 (2001).
- Zhang, X. B. *et al.* Detection of human influence on twentieth-century precipitation trends. *Nature*. **448**, 461–465 (2007).
- Chan, C. L. Tropical cyclone activity over the western North Pacific associated with El Niño and La Niña events. *J. Clim.* **13**, 2960–2972 (2000).
- Yeh, S. W. *et al.* El Niño in a changing climate. *Nature*. **461**, 511–514 (2009).
- Ding, Y., Wang, Z. & Sun, Y. Inter-decadal variation of the summer precipitation in East China and its association with decreasing Asian summer monsoon. Part I: Observed evidences. *Int. J. Clim.* **28**, 1139–1161 (2008).
- Bollasina, A., Ming, Y. & Ramaswamy, V. Anthropogenic aerosols and the weakening of the South Asian summer monsoon. *Science*. **334**, 502–505 (2011).
- Rajendran, K., Nanjundiah, R. S., Gadgil, S. & Srinivasan, J. How good are the simulations of tropical SST-rainfall relationship by IPCC AR4 atmospheric and coupled models? *J. Earth. Syst. Sci.* **121**, 595–610 (2012).
- Haywood, J. & Boucher, O. Estimates of the direct and indirect radiative forcing due to tropospheric aerosols: A review. *Rev. Geophys.* **38**, 513–543 (2000).
- Menon, S., Hansen, J., Nazarenko, L. & Luo, Y. Climate effects of black carbon aerosols in China and India. *Science*. **297**, 2250–2253 (2002).
- Wentz, F. J., Ricciardulli, L., Hilburn, K. & Mears, C. How much more rain will global warming bring? *Science*. **317**, 233–235 (2007).
- Xie, S. P., Lu, B. & Xiang, B. Similar spatial patterns of climate responses to aerosol and greenhouse gas changes. *Nature Geosci.* **6**, 828–832 (2013).
- Adler, R. F. *et al.* The version-2 global precipitation climatology project (GPCP) monthly precipitation analysis (1979–present). *J. Hydrometeorol.* **4**, 1147–1167 (2003).
- Bolvin, D. T. *et al.* Comparison of GPCP Monthly and Daily Precipitation Estimates with High-Latitude Gauge Observations. *J. Appl. Meteorol. Clim.* **48**, 1843–1857 (2009).
- Smith, T. M., Reynolds, R. W., Peterson, T. C. & Lawrimore, J. Improvements to NOAA’s historical merged land-ocean surface temperature analysis (1880–2006). *J. Clim.* **21**, 2283–2296 (2008).
- Kumar, O. B., Naidu, C. V. & Rao, S. R. L. Influence of southern oscillation and SSTs over Niño-3.4 region on the winter monsoon rainfall over coastal Andhra Pradesh. *J. Earth. Syst. Sci.* **113**, 313–319 (2004).
- Li, J. & Zeng, Q. A unified monsoon index. *Geophys. Res. Lett.* **29**, 115-1–115-4 (2002).
- Li, J. & Zeng, Q. A new monsoon index and the geographical distribution of the global monsoons. *Adv. Atmos. Sci.* **20**, 299–302 (2003).
- Wang, B. & Fan, Z. Choice of South Asian summer monsoon indices. *B. Am. Meteorol. Soc.* **80**, 629–638 (1999).
- Wang, B., Wu, R. & Lau, K. Interannual variability of Asian summer monsoon: Contrast between the Indian and western North Pacific-East Asian monsoons. *J. Clim.* **14**, 4073–4090 (2001).
- XIA, N. A., Chen, H. B. & Wang, P. C. Validation of MODIS aerosol retrievals and evaluation of potential cloud contamination in East Asia. *J. Environ. Sci.* **16**, 832–837 (2004).
- Xin, J. *et al.* Aerosol optical depth (AOD) and Angström exponent of aerosols observed by the Chinese Sun Hazemeter Network from August 2004 to September 2005. *J. Geophys. Res.* **112**, D05203 (2007).
- Kalnay, E. *et al.* The NCEP/NCAR 40-year reanalysis project. *B. Am. Meteorol. Soc.* **77**, 437–471 (1996).
- Xue, X. F., Song, Z. W., Amrine, J. W. & Hong, X. Y. Eriophyid mites (Acari: Eriophyoidea) on bamboo from China, with descriptions of three new species from the Qinling Mountains. *Ann. Entomol. Soc. Am.* **99**, 1057–1063 (2006).
- North, G. R. Empirical orthogonal functions and normal modes. *J. Atmos. Sci.* **41**, 879–887 (1984).
- Dai, A., Funk, I. Y. & Del Genio, A. D. Surface observed global land precipitation variations during 1900–88. *J. Clim.* **10**, 2943–2962 (1997).
- Shaw, S. B., Royem, A. A. & Riha, S. J. The relationship between extreme hourly precipitation and surface temperature in different hydroclimatic regions of the United States. *J. Hydrometeorol.* **12**, 319–325 (2011).
- Kim, Y. S., Kwon, B. H. & Hong, K. M. ESTIMATION OF THE AIR TEMPERATURE OVER THE OCEAN BASED ON SATELLITE DATA. *Gayana (Concepción)*. **68**, 317–318 (2004).
- Susan, S. *et al.* Climate Change 2007-The Physical Science Basis: Working Group I Contribution To The Fourth Assessment Report Of The IPCC. *Cambridge Univ. Press*. (2007).
- Smith, T. M., Yin, X. & Gruber, A. Variations in annual global precipitation (1979–2004), based on the Global Precipitation Climatology Project 2.5 analysis. *Geophys. Res. Lett.* **33**, L6705 (2006).
- Trenberth, K. E., Fasullo, J. & Smith, L. Trends and variability in column-integrated atmospheric water vapor. *Clim. Dynam.* **24**, 741–758 (2005).
- Ju, J. & Slingo, J. The Asian summer monsoon and ENSO. *Q. J. Roy. Meteor. Soc.* **121**, 1133–1168 (1995).
- Gu, G. & Adler, R. F. Interdecadal variability/long-term changes in global precipitation patterns during the past three decades: global warming and/or pacific decadal variability? *Clim. Dynam.* **40**, 3009–3022 (2013).
- Westra, S., Alexander, L. V. & Zwiars, F. W. Global increasing trends in annual maximum daily precipitation. *J. Clim.* **26**, 3904–3918 (2013).
- Emori, S. & Brown, S. J. Dynamic and thermodynamic changes in mean and extreme precipitation under changed climate. *Geophys. Res. Lett.* **32**, L17706 (2005).
- Wijngaard, J. B., Klein Tank, A. M. G. & Können, G. P. Homogeneity of 20th century European daily temperature and precipitation series. *Int. J. Clim.* **23**, 679–692 (2003).
- Bond, N. A., Overland, J. E., Spillane, M. & Stabeno, P. Recent shifts in the state of the North Pacific. *Geophys. Res. Lett.* **30**, 2183 (2003).
- Adler, R. F. *et al.* Relationships between global precipitation and surface temperature on interannual and longer timescales (1979–2006). *J. Geophys. Res. Atmospheres*. **113**, D22104 (2008).
- Ma, Z. G. The interdecadal trend and shift of dry/wet over the central part of North China and their relationship to the Pacific Decadal Oscillation (PDO). *Chinese Sci. Bull.* **52**, 2130–2139 (2007).
- Zou, X., Zhai, P. & Zhang, Q. Variations in droughts over China: 1951–2003. *Geophys. Res. Lett.* **32**, L04707 (2005).
- Rosenfeld, D. *et al.* Flood or drought: how do aerosols affect precipitation? *Science*. **321**, 1309–1313 (2008).
- Koren, I. *et al.* Aerosol-induced intensification of rain from the tropics to the mid-latitudes. *Nature Geosci.* **5**, 118–122 (2012).
- Yi, B., Yang, P., Bowman, K. P. & Liu, X. Aerosol-cloud-precipitation relationships from satellite observations and global climate model simulations. *J. Appl. Remote Sens.* **6**, 63501 (2012).
- Tang, J. *et al.* Positive relationship between liquid cloud droplet effective radius and aerosol optical depth over Eastern China from satellite data. *Atmos. Environ.* **84**, 244–253 (2013).



53. Liu, X.-H. *et al.* Understanding of regional air pollution over China using CMAQ, part II. Process analysis and sensitivity of ozone and particulate matter to precursor emissions. *Atmos. Environ.* **44**, 3719–3727 (2010).

## Acknowledgments

This study is supported by 2014CB953700 and NFSC 41176099. We thank National Aeronautics and Space Administration (NASA) and National Oceanic and Atmospheric Administration (NOAA) for the data service.

## Author contributions

D.Y. wrote the main manuscript text, G.H., Y.X. and X.L. modified it, G.T. prepared figures 3, 4 and supplementary figure S1, S2. All authors reviewed the manuscript.

## Additional information

**Supplementary information** accompanies this paper at <http://www.nature.com/scientificreports>

**Competing financial interests:** The authors declare no competing financial interests.

**How to cite this article:** Deng, Y.Y., Gao, T., Gao, H.W., Yao, X.H. & Xie, L. Regional precipitation variability in East Asia related to climate and environmental factors during 1979–2012. *Sci. Rep.* **4**, 5693; DOI:10.1038/srep05693 (2014).



This work is licensed under a Creative Commons Attribution-NonCommercial-NoDerivs 4.0 International License. The images or other third party material in this article are included in the article's Creative Commons license, unless indicated otherwise in the credit line; if the material is not included under the Creative Commons license, users will need to obtain permission from the license holder in order to reproduce the material. To view a copy of this license, visit <http://creativecommons.org/licenses/by-nc-nd/4.0/>